Nanoscale Res Lett (2008) 3:152–157
DOI 10.1007/s11671-008-9129-1

NANO EXPRESS

Effect of Variations in Annealing Temperature and Metallic Cations on Nanostructured Molybdate Thin Films

Ana Paula de Azevedo Marques · Edson Roberto Leite · José Arana Varela · Elson Longo

Received: 17 January 2008 / Accepted: 26 March 2008 / Published online: 29 April 2008

Abstract Crystalline molybdate thin films were prepared by the complex polymerization method. The $AMoO_4$ (A = Ca, Sr, Ba) films were deposited onto Si wafers by the spinning technique. The Mo–O bond in the $AMoO_4$ structure was confirmed by FTIR spectra. X-ray diffraction revealed the presence of crystalline scheelite-type phase. The mass, size, and basicity of A^{2+} cations was found to be dependent on the intrinsic characteristics of the materials. The grain size increased in the following order: $CaMoO_4 < SrMoO_4 < BaMoO_4$. The emission band wavelength was detected at around 576 nm. Our findings suggest that the material's morphology and photoluminescence were both affected by the variations in cations (Ca, Sr, or Ba) and in the thermal treatment.

Keywords Molybdates · Thin films · Complex polymerization method

Introduction

Molybdates with scheelite-type structures (tetragonal C_{4h}^6 symmetry) are able to produce green luminescence. These compounds have attracted much attention due to their application as phosphors and as scintillating materials in electrooptical applications like solid-state lasers and optical fibers [1, 2].

A. P. A. Marques (✉) · E. R. Leite · E. Longo
LIEC-CMDMC, DQ, UFSCar, Via Washington Luiz, km 235, CEP 13565-905 Sao Carlos, SP, Brazil
e-mail: apamarques@power.ufscar.br

J. A. Varela · E. Longo
LIEC-CMDMC, IQ, UNESP, Rua Francisco Degni s/n, CEP 14800-900 Araraquara, SP, Brazil

Molybdates thin films have a wide variety of applications in electronics, optics, ionics, and anticorrosive coatings. A great deal of interest has focused on the preparation of molybdate thin films due to their optical properties and nanometric scale [3–6].

$BaMO_4$ (BMO), $SrMO_4$ (SMO), and $CaMO_4$ (CMO) powders with a scheelite structure have been synthesized by a variety of techniques, including combustion synthesis, the Czochralski technique, co-precipitation by conventional solid-state reaction, and the complex polymerization method (CPM) [1, 5–9]. However, references in the literature about the synthesis of $AMoO_4$ (AMO) thin films are rare and the most commonly cited method is the electrochemical route [3, 10–12]. The electrochemical method is limited because it uses only Mo substrates to prepare AMO films [13].

Another limitation of the electrochemical method is its lack of homogeneity. BMO thin films produced by an electrochemical method showed a heterogeneous surface and grain sizes varying from 2 to 10 μm [12]. When the CPM is used, the metal complexes become immobilized in a rigid organic polymeric network, reducing the segregation of particular metals and thus ensuring compositional homogeneity on a molecular scale [6]. The additional advantage of CPM is that it does not require expensive equipment or reagents, deposition in high vacuum chambers or special atmospheric control.

The $[MoO_4]^{2-}$ ionic group in the AMO scheelite structure, which has strong covalent Mo–O bonds, is coupled to Ca^{2+}, Sr^{2+}, or Ba^{2+} cations [4–7]. Many authors attribute the photoluminescent property in these materials to the MoO_4^{2-} cluster and its possible intermediary states ($MoO_4 \cdots O \cdot MoO_3$, $MoO_4 \cdots O \cdots MoO_4$) [5–7, 14]. Because the property of photoluminescence (PL) is associated with distortion in tetrahedra, it is reasonable to assume that PL can be affected by metallic cations.

In the present work, we evaluated the effects on molybdate thin films resulting from variations in the metallic cations and thermal treatment. Crystalline AMO thin films were prepared by the CPM, and were characterized by various techniques, such as X-ray diffraction (XRD), optical reflectance spectroscopy (ORS), Fourier transform infrared reflectance (FTIR), atomic force microscopy (AFM), high-resolution scanning electron microscopy (HR-SEM), and photoluminescence spectroscopy (PLS).

Experimental Procedure

Materials

The materials used in this study were molybdenum trioxide MoO_3 (Synth 85%), $BaCO_3$, $SrCO_3$, and $BaCO_3$ (Mallinckrodt 99%), citric acid ($H_3C_6H_5O_7$) (Mallinckrodt 99%) and ethylene glycol ($HOCH_2CH_2OH$) (J. T. Baker 99%). All the chemicals were used without further purification.

Preparation of AMO Thin Films (A = Ca^{2+}, Sr^{2+}, Ba^{2+})

AMO thin films were produced by deposition of the polymeric resin obtained by CPM onto Si substrates. In this synthesis, the molybdenum citrate was formed by dissolving molybdic acid (MoO_3—molybdenum trioxide) in an aqueous solution of citric acid under constant stirring at 60–80 °C to homogenize the molybdenum citrate solution (the molar ratio of citric acid to molybdic acid was 6:1). The solution was homogenized, after which the metallic carbonate (Ca^{2+}, Sr^{2+}, and Ba^{2+}) was dissolved and a stoichiometric amount added to the molybdenum citrate solution. The complex was stirred thoroughly for several hours at 60–80 °C to produce a clear and homogeneous solution. Ethylene glycol was then added to polymerize the citrate by polyesterification. The viscosity of the solution increased under continual heating at 80–90 °C, although no phase separation was detected. The molar ratio of metallic cations to molybdenum cations was 1:1. The citric acid/ethylene glycol mass ratio was set at 60:40. The viscosity of the deposition solution was adjusted to 15 mPa/s by controlling the water content.

A total of six thin films were produced using Si(100) wafers as substrates. The substrates were spin-coated by dropping a small amount of the polymeric resin onto them. Rotation speed and spin time were fixed at 700 rpm for 3 s and 7200 rpm for 30 s, using a commercial spinner (Chemat Technology KW-4B spin-coater). After deposition, the films were heat-treated at 80 °C for 30 min, 100 °C for 20 min and 200 °C for 2 h, applying a heating rate of 1 °C/min. Four layers were deposited and the procedure was repeated for each layer. In the last layer, after the heat treatment at 200 °C, two different crystallization procedures were applied, one involving heat treatments at 600 °C for 2 h in a resistance furnace (RF) and the other at 600 °C for 10 min in a microwave (MW) oven.

Characterization of AMO Thin Films

The AMO thin films were characterized by XRD, using Cu $K\alpha$ radiation to determine the resulting phases. The optical reflectance was measured in the wavelength range of 200–800 nm, using a UV–vis–NIR Cary 5G spectrophotometer. Fourier transform infrared reflectance spectra for thin films were recorded in the frequency range of 400–2100 cm^{-1} at room temperature, using an Equinox/55 (Bruker) spectrometer equipped with a 30° specular reflectance accessory. A reconstructed 3D image of the surface of the sample was obtained by atomic force microscopy (AFM), using a Digital Instruments Multi-Mode Nanoscope IIIa microscope. This type of image allows for accurate analysis and quantification of highly relevant parameters such as roughness and grain size. The microstructure and surface morphology of the thin films were observed by high resolution scanning electron microscopy (HR-SEM), using a field emission gun (Gemini-Zeiss Supra35). Photoluminescence spectra of AMO thin films were recorded with a Jobin Yvon-Fluorolog spectrofluorometer coupled to a 450 W xenon lamp. All the measurements were taken at room temperature.

Results and Discussion

Figure 1 shows X-ray patterns of AMO thin films deposited onto Si substrates after heat treatment at 600 °C in the

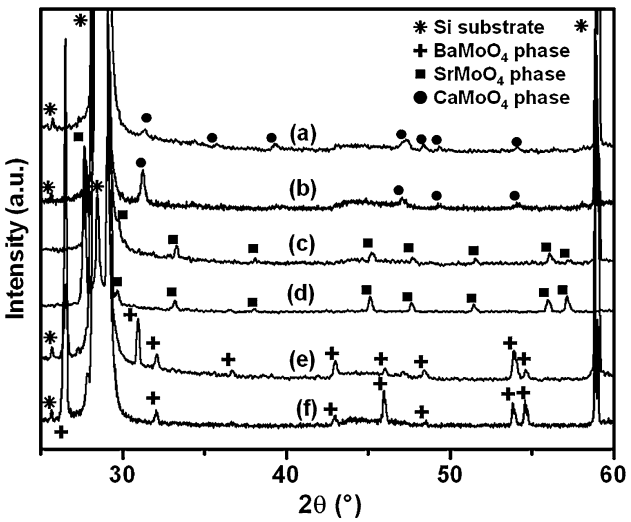

Fig. 1 X-ray diffraction patterns of AMO thin films deposited on Si(100) and heat-treated at 600 °C for 10 min in a MW oven and for 2 h in a RF. CMO-MW (**a**), CMO-RF (**b**), SMO-MW (**c**), SMO-RF (**d**), BMO-MW (**e**), and BMO-RF (**f**)

Table 1 Lattice constants and cell volume of the tetragonal structure of AMO thin films

Thin films	Lattice constants (Å) [15]		Lattice constants (Å)[a]		Cell volume (Å^3) [15]	Cell volume (Å^3)[a]
	a	*c*	*a*	*c*		
BMO^{RF}	5.580	12.821	5.582 (2)	12.775 (8)	399.20	398.06
BMO^{MW}	5.580	12.821	5.580 (5)	12.816 (23)	399.20	399.04
SMO^{RF}	5.394	12.020	5.395 (3)	12.045 (15)	349.72	350.58
SMO^{MW}	5.394	12.020	5.390 (1)	12.012 (5)	349.72	348.97
CMO^{RF}	5.226	11.430	5.223 (11)	11.397 (36)	312.17	310.91
CMO^{MW}	5.226	11.430	5.219 (2)	11.422 (6)	312.17	311.11

[a] Our data

RF AMO thin film heat-treated at 600 °C/2 h in resistive furnace

MW AMO thin film heat-treated at 600 °C/10 min in MV

RF and MW oven. The diffraction peak (112) (100% peak), 2θ at around 28.8°, indicated the formation of crystalline scheelite-type phase. The diffraction peaks were indexed according to the JCPDS data base nos. 29–0193, 08–0482 and 29–0351 for the $BaMoO_4$, $SrMoO_4$, and $CaMoO_4$ thin films, respectively, confirming the sole presence of scheelite phase in all the thin films [1, 15, 16]. In both $CaMoO_4$ thin films, the diffraction peak (112) occurred in the same 2θ region of Si substrate, 2θ at around 28.8°, thus indicating the occurrence of overlapping. However, the other diffraction peaks confirm the formation of the desired phase. The lattice parameters of the thin films were estimated by the least-squares refinement program REDE93 and are presented in Table 1. These values are highly congruent with others reported in the literature [15]. We confirmed that the lattice parameters *a* and *c*, the cell volume and the unit-cell parameters of AMO decreased linearly as the ionic radius of the cations decreased. The ionic radius of Ca^{2+} (0.120 nm) is smaller than those of Sr^{2+} and Ba^{2+} (0.132 and 0.149 nm, respectively). This difference led to lattice parameters that were low for CMO, intermediary for SMO and high for BMO thin films.

Figure 2 shows FTIR spectra and Table 2 presents data on the $F_2(v_3)$ vibrations of crystalline AMO thin films. The tetrahedral symmetry is represented by: $\Gamma_{Td} = A_1(v_1) + E(v_2) + F_2(v_3) + F_2(v_4)$, but only the $F_2(v_3, v_4)$ modes are active in infrared. The $F_2(v_3)$ vibrations are antisymmetric stretches, whereas the $F_2(v_4)$ vibrations are bending modes. Therefore, the bands between 820 and 796 cm^{-1} were assigned to $F_2(v_3)$ antisymmetric stretching vibrations of thin films heat-treated at 600 °C. These bands reportedly correspond to the Mo–O stretching vibration in the MoO_4^{2-} tetrahedron [17]. In this work, we found that the $F_2(v_3)$ antisymmetric stretching vibrations occurred in the following order: $Ca^{2+} < Sr^{2+} < Ba^{2+}$. This observation is congruent with that of Basiev et al., who reported the dependence of the vibrational spectra of scheelite crystals on the mass, size, and basicity of A^{2+} cations [4]. Basiev identified this dependence by Raman spectroscopy, and in this work we observed it by IR spectroscopy.

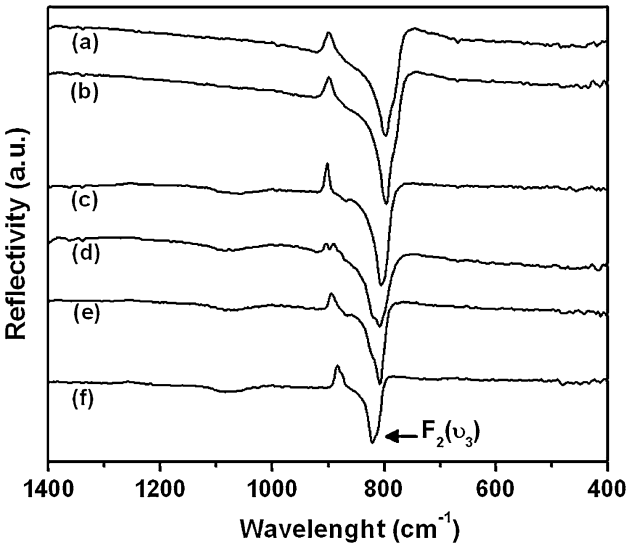

Fig. 2 FTIR spectra of AMO thin films: CMO-MW (**a**), CMO-RF (**b**), SMO-MW (**c**), SMO-RF (**d**), BMO-MW (**e**), and BMO-RF (**f**)

Table 2 $F_2(v_3)$ vibration in FTIR absorption spectra of AMO thin films

Thin films	Vibrations $F_2(v_3)$ (cm^{-1})
BMO^{RF}	820
BMO^{MW}	809
SMO^{RF}	808
SMO^{MW}	804
CMO^{RF}	796
CMO ^{MW}	798

RF AMO thin film heat-treated at 600 °C/2 h in resistive furnace

MW AMO thin film heat-treated at 600 °C/10 min in MV

Figures 3 and 4 show HR-SEM micrographs of the cross section and surface, respectively, of AMO thin films. The

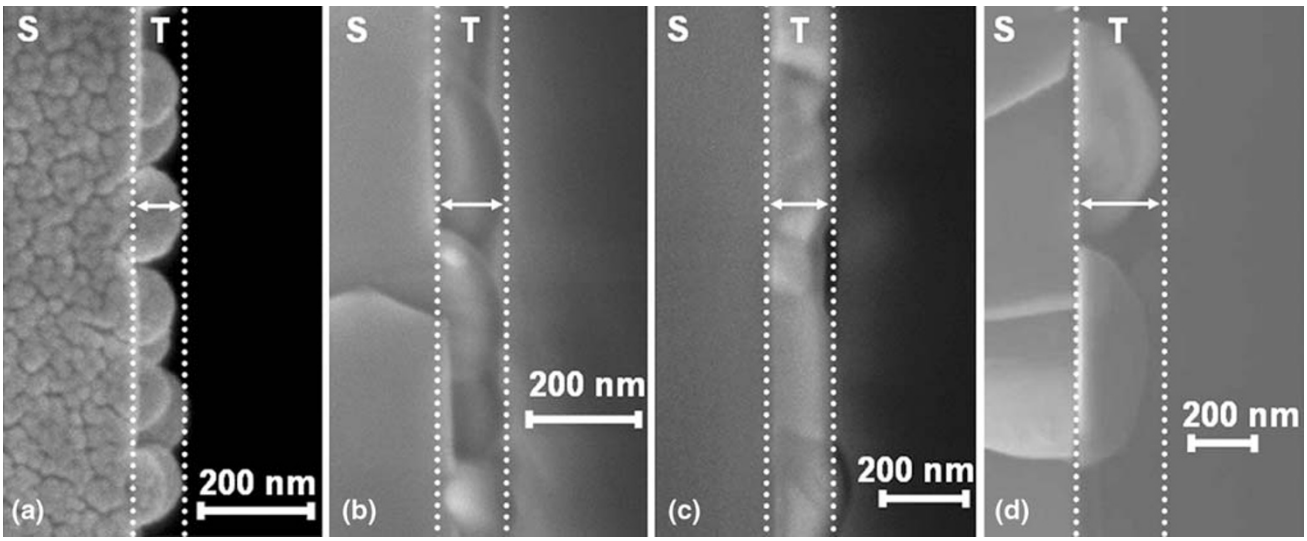

Fig. 3 HR-SEM micrograph showing the thickness of AMO thin films: CMO-MW (**a**), SMO-MW (**b**), BMO-MW (**c**), and BMO-RF (**d**)

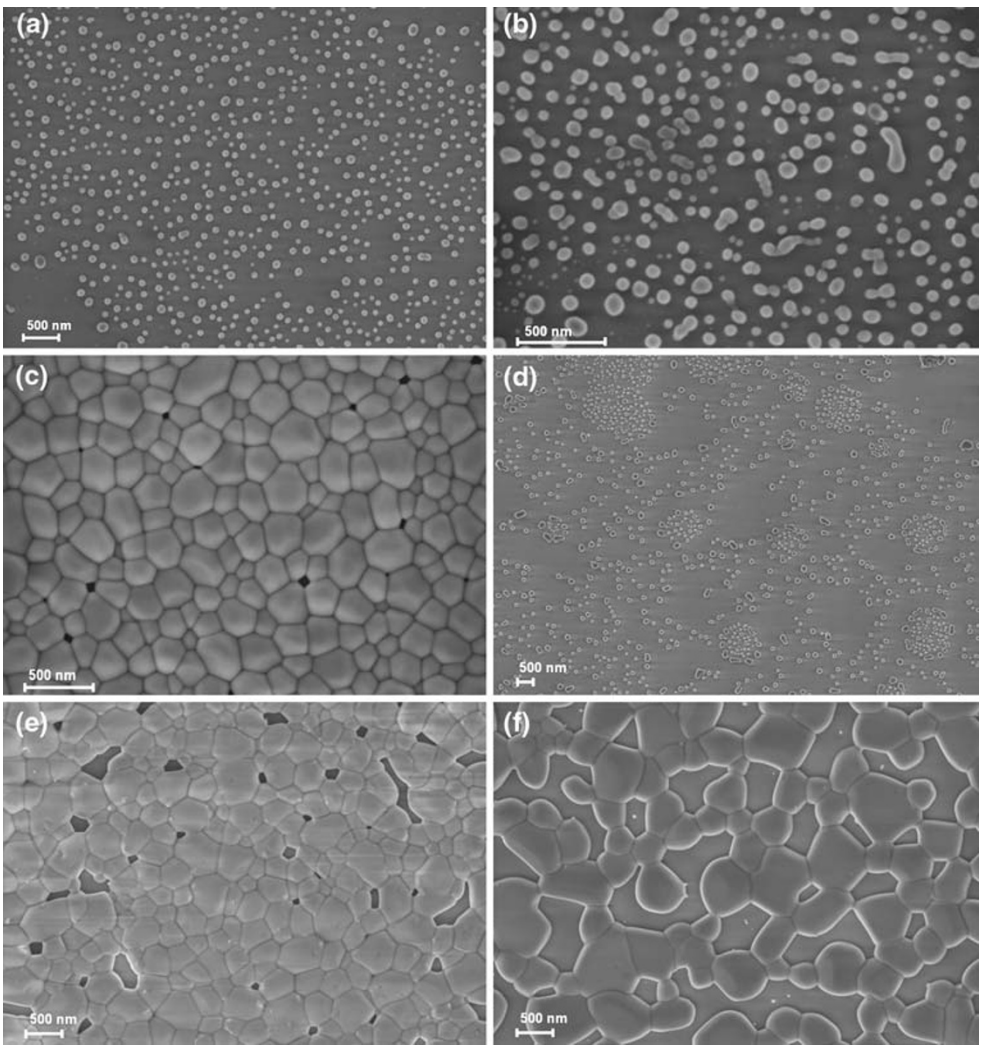

Fig. 4 HR-SEM micrograph of the surface of AMO thin films: CMO-MW (**a**) CMO-RF (**b**), SMO-MW (**c**), SMO-RF (**d**), BMO-MW (**e**), and BMO-RF (**f**)

BMO thin films treated at 600 °C for 2 h in the RF were about 484 nm thick, while the SMO films were 109 nm thick. The BMO, SMO, and CMO thin films treated at 600 °C for 10 min in the MW oven showed thicknesses of about 164, 129, and 107 nm, respectively. The thickness of the CMO thin film heat-treated in the MW oven was estimated, since the material had to be coated with a gold layer before taking this measurement.

As can be seen in Fig. 4, the thin films heat-treated in the RF and the MW showed distinct morphologies. The thin film heat-treated in the MW tended to be continuous, while the film treated in the RF tended to form nanoislands. This is probably because the temperature in the RF rises more slowly than in the MW. The slow increase in temperature facilitates shrinking of the polymeric resin on the substrate surface, giving rise to nanoisland structures. Because the nanoisland structures were extremely thin, it was difficult to see the thickness of thin films heat-treated in the RF, and we were unable to ascertain the thickness of the $CaMoO_4$ thin film heat-treated in the RF.

The micrographs indicate that the thickness, grain size, and type of morphology are dependent on the metallic cations and the heat treatment history. The lattice constants and cell volume of the tetragonal structure of AMO thin films revealed by X-ray diffraction decreased linearly with a diminishing ionic radius. Therefore, the grain size is expected to increase in the following order: CMO < SMO < BMO. As expected, the grain sizes were about 78.38, 83.18, and 133.25 nm, respectively, for CMO, SMO, and BMO thin films. The thickness proved to be dependent on the grain size; therefore, it followed the same order of growth. The morphological structure was devoid of cracks, homogeneous, and distinct in all the films.

The AFM analysis (Fig. 5) showed that the morphology of the thin films was homogenous, with BMO, SMO, and CMO showing grain sizes of about 300, 190, and 170 nm, respectively, which is congruent with the characteristics depicted in the HR-SEM micrographs (Fig. 4). The SMO thin films displayed the lowest roughness, i.e., about 108 nm, which was expected because of the continuous surface morphology of these films. The CMO films showed the highest roughness, i.e., about 349 nm, because of their nanoisland structure, which increased their roughness. The BMO thin films showed a roughness of about 213 nm.

Figure 6 depicts reflectivity spectra recorded in the range of 2.0–6.0 eV for the AMO thin films, showing two bands, one near 3.38 (367 nm) and the other at 4.38 eV (283 nm). Spassky et al. attributed the band at 4.38 eV to electronic transitions within the MoO_4^{2-} complex. The band observed at around 3.38 eV corresponds to the creation of the excitonic state in A^{2+}, where A = Ba, Sr, or Ca [9].

Figure 7 illustrates PL spectra of the crystalline AMO thin films recorded at room temperature. The samples were excited by the 330 nm line of a 450 W xenon lamp. The band emission wavelength of the AMO thin films was located at about 576 nm. The solely green emission is an

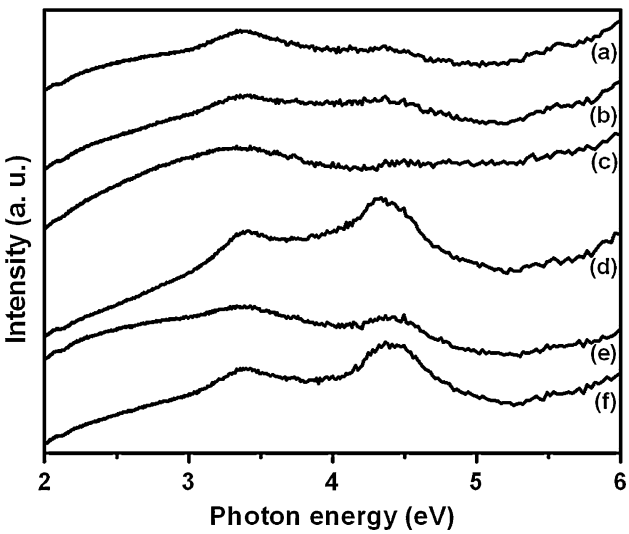

Fig. 6 Reflectivity spectra of AMO thin films recorded in the range of 2.0–6.0 eV: CMO-MW (**a**) CMO-RF (**b**), SMO-MW (**c**), SMO-RF (**d**), BMO-MW (**e**), and BMO-RF (**f**)

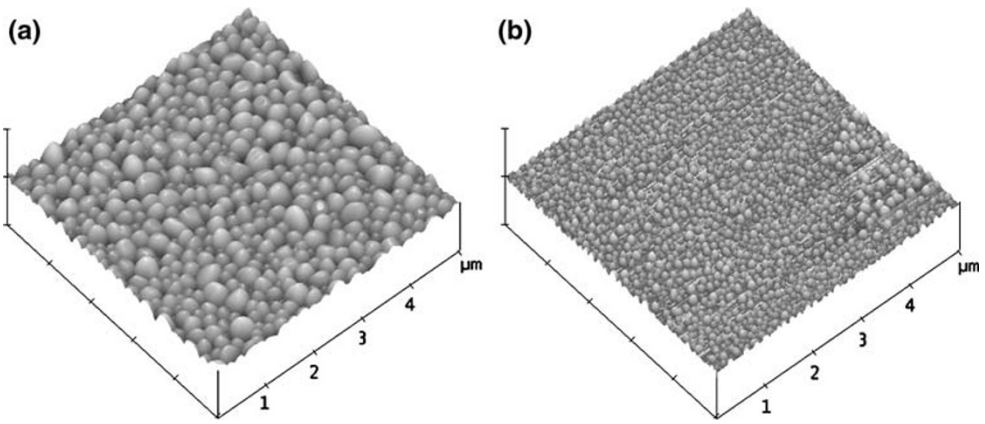

Fig. 5 AFM 3D images of the surfaces of SMO-RF (**a**) and CMO-MW (**b**)

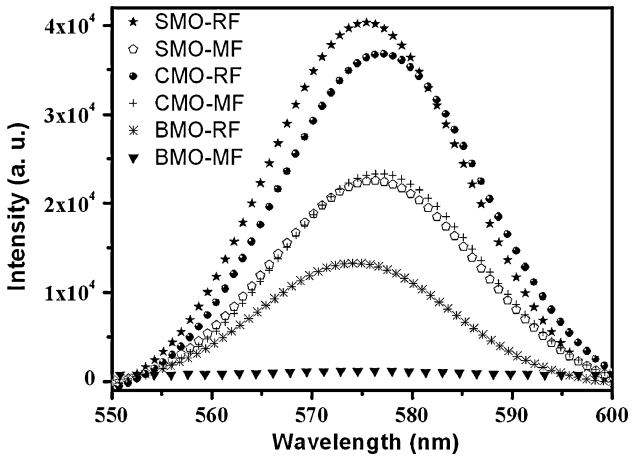

Fig. 7 Room-temperature emission spectra of the $BaMoO_4$ (BMO), $SrMoO_4$ (SMO), and $CaMoO_4$ (CMO) thin films deposited on Si(100) and heat-treated at 600 °C in a RF and in a MF oven. $\lambda_{Exc.}$ = 330 nm

important feature, suggesting that the thin films are defect-free [10]. The BMO thin films heat-treated in the MW oven emitted practically no PL. The PL property is associated with the history of thermal treatment and the metallic cations in the films, and thus, with the crystalline structure. Many authors attribute the PL property in scheelite-type materials to the MoO_4^{2-} cluster and its possible intermediary states ($MoO_4 \cdots O \cdot MoO_3$, $MoO_4 \cdots O \cdots MoO_4$). Hence, it is reasonable to suppose that metallic cations such as Ca^{2+}, Sr^{2+}, and Ba^{2+}, which are lattice-modifying agents, also affect the PL property [5–7, 14]. Our group is engaged in studies aimed at shedding further light on the relation between luminescent properties and metallic cations, based on theoretical calculations, and our findings will be published when they become available.

Conclusions

The crystalline scheelite-type phase was confirmed in the BMO, SMO, and CMO thin films using the aforementioned characterization techniques. Processing thin films by CPM proved efficient and involved little cost, since this method does not require expensive equipment or reagents, deposition in high vacuum chambers or special atmospheric control. The mass, size, and basicity of the A^{2+} cation was found to be dependent on the intrinsic characteristics of the materials. Our findings suggest that both the morphology and the PL of the material are affected by variations in the cations (Ca, Sr, or Ba) and in the thermal treatment. These results confirmed that AMO thin films are highly promising candidates for PL applications.

Acknowledgments This work was supported by CNPq, FAPESP-CEPID, and CAPES.

References

1. J.H. Ryu, J.W. Yoon, C.S. Lim, W.C. Oh, K.B. Shim, J. Alloys Compod. **390**, 245 (2005)
2. N. Klassen, S. Shmurak, B. Red'kin, B. Ille, M. Lebeau, P. Lecoq, M. Schneegans, Nucl. Instrum. Methods Phys. Res., Sect. A Accelerat. Spectr. Detect. Assoc. Equip. **486**, 431 (2002)
3. W.S. Cho, M. Yashima, M. Kakihana, A. Kudo, T. Sakata, M. Yoshimura, J. Am. Ceram. Soc. **80**, 765 (1997)
4. T.T. Basiev, A.A. Sobol, Y.K. Voronko, P.G. Zverev, Opt. Mater. **15**, 205 (2000)
5. A.P.D. Marques, D.M.A. de Melo, C.A. Paskocimas, P.S. Pizani, M.R. Joya, E.R. Leite, E. Longo, J. Solid State Chem. **179**, 671 (2006)
6. A.P.A. Marques, D.M.A. de Melo, E. Longo, C.A. Paskocimas, P.S. Pizani, E.R. Leite, J. Solid State Chem. **178**, 2346 (2005)
7. A.P. de Azevedo Marques, E.R. Dockal, F.C. Skrobot, I.L. Viana Rosa, Inorg. Chem. Commun. **10**, 255 (2007)
8. F.A. Kroger, *Some Aspects of the Luminescence of Solids* (Elsevier, Amsterdam, 1948), p. 107; G. Hitoki, T. Takata, S. Ikeda, M. Hara, J.N. Kondo, M. Kakihana, K. Domen, Catal. Today **63**, 175 (2000); M.A. Hasan, M.I. Zaki, K. Kumari, L. Pasupulety, Thermochim. Acta **320**, 23 (1998)
9. D.A. Spassky, S.N. Ivanov, V.N. Kolobanov, V.V. Mikhailin, V.N. Zemskov, B.I. Zadneprovski, L.I. Potkin, Radiat. Meas. **38**, 607 (2004)
10. M. Yoshimura, M. Ohmura, W.S. Cho, M. Yashima, M. Kakihana, J. Am. Ceram. Soc. **80**, 2464 (1997)
11. C.T. Xia, V.M. Fuenzalida, R.A. Zarate, J. Alloys Compod. **316**, 250 (2001)
12. C.T. Xia, V.M. Fuenzalida, J. Europ. Ceram. Soc. **23**, 519 (2003)
13. H. Lei, X. Zhu, Y. Sun, W. Song, J. Cryst. Growth **310**, 789 (2008)
14. M.A.M.A. Maurera, A.G. Souza, L.E.B. Soledade, F.M. Pontes, E. Longo, E.R. Leite, J.A. Varela, Mater. Lett. **58**, 727 (2004)
15. JCPDS No 29-0193, JCPDS No 08-0482, JCPDS No 29-0351
16. V. Thangadurai, C. Knittlmayer, W. Weppner, Mater. Sci. Eng. B Solid State Mater. Adv. Technol. **106**, 228 (2004)
17. K. Nakamoto, *Infrared and Raman Spectra of Inorganic and Coordination Compounds* (Wiley, New York, 1986)